J Solid State Electrochem
DOI 10.1007/s10008-017-3735-8

ORIGINAL PAPER

Underpotential deposition and involved alloy formation of cadmium on silver particles modified HOPG substrates

Rubén E. Ambrusi[1] · **María E. Pronsato**[2] · **Silvana G. García**[1]

Received: 20 February 2017 / Revised: 7 August 2017 / Accepted: 14 August 2017

Abstract Cadmium underpotential deposition (UPD) on Ag particles modified highly ordered pyrolytic graphite (HOPG) surfaces, and the involved alloy formation were studied by conventional electrochemical techniques. Voltammetric results indicated that the Cd UPD followed an adsorption behavior different from that observed for massive Ag electrodes and Ag particles supported on vitreous carbon. Nanometer-sized bimetallic Cd–Ag particles were characterized by ex situ atomic force microscopy (AFM). Initially, AFM images show Ag deposits of similar size distributed preferably on HOPG step edges. No remarkable morphological changes are observed on the surface after the subsequent Cd deposition, suggesting that the Cd particles are deposited selectively over the Ag crystals. From the analysis of desorption spectra, employing different polarization times, and density functional theory (DFT) calculations, the formation of a Cd–Ag surface alloy could be inferred.

Keywords Bimetallic particles · Underpotential deposition · Electrodeposition · Cd–Ag alloy · Density functional theory

Electronic supplementary material The online version of this article (https://doi.org/10.1007/s10008-017-3735-8) contains supplementary material, which is available to authorized users.

✉ Silvana G. García
sgarcia@criba.edu.ar

[1] Instituto de Ingeniería Electroquímica y Corrosión (INIEC), Departamento de Ingeniería Química, Universidad Nacional del Sur, Av. Alem 1253, 8000 Bahía Blanca, Argentina

[2] Instituto de Física del Sur (IFISUR), Departamento de Física, Universidad Nacional del Sur, Av. Alem 1253, 8000 Bahía Blanca, Argentina

Introduction

It has been demonstrated that the electrodeposition is one of the most promising methods to prepare well-dispersed and uniform Ag particles on carbon substrates like vitreous carbon (VC) [1, 2] and highly ordered pyrolytic graphite (HOPG) [3–7], from different plating solutions, selecting adequate polarization conditions. For this reason, these modified carbon electrodes may be used as substrates for the subsequent deposition of other metal.

On the other hand, the synthesis of bimetallic nanoparticles composed of two different metal elements has attracted increasing interest due to improved catalytic performance as a result of the synergistic and electronic effects which are different from those of monometallic analogues [8–10]. Especially, this study focuses on the generation of Cd–Ag bimetallic nanostructures because they have interesting catalytic properties toward the nitrate anions reduction reaction, which are contaminants of effluents. The catalytic effect of this type of structures was demonstrated qualitatively for Cd/Ag films on Au single crystal electrodes [11], and for bimetallic Cd–Ag nanoparticles on vitreous carbon (VC) substrates [12].

Particularly, the preparation of bimetallic nanoparticles by electrochemical methods is usually based on the "avalanche nucleation" phenomenon described by Deutscher and Fletcher [13]. These authors have demonstrated that the addition of trace concentrations of a more reduced metal to a plating solution containing a less easily reduced metal caused an increase in the nucleation rate of the later. In the case of Ag particles, this approach was also used by Penner et al. [14] to deposit selectively Cu on Ag particles supported on graphite.

In our case, the application of this method is favored by the fact that Cd presents the underpotential deposition (UPD)

Published online: 25 August 2017

phenomenon on Ag electrodes, which was already studied through electrochemical measurements and in situ scanning tunneling microscope (STM) [15–19]. The UPD process is referred as the electrodeposition of 1–2 monolayers or submonolayers of a metal (Me) on a foreign substrate (S) at potentials more positive than the Nernst equilibrium potential of the three-dimensional (3D) metal bulk phase (E_{3DMe}) [20, 21]. A previous work of Cd/Ag crystals on vitreous carbon (VC) electrodes was obtained exploiting this property [22]. In this case, the Cd UPD process was evidenced by only an adsorption current peak before the massive Cd deposition.

Based on the mixing pattern of the two constituent elements, the bimetallic pair can be distributed forming a random "alloy," a "core-shell" structure, or an "oligomer" (structures ensemble each of them composed of pure metal component) [14]. According to the literature, the occurrence of an alloy between Cd and Ag was demonstrated in the UPD range, for mono- and polycrystalline Ag electrodes [15, 18, 19], and for Ag nanoparticles on VC [22]. Therefore, it is expected that this phenomenon will also take place in the Cd–Ag/HOPG system. This feature is very important because the synergistic effect between Ag and Cd to catalyze the reduction of nitrate anions may be enhanced by the alloy structure.

On the other hand, using a support like HOPG is particularly important due to its stepped structure, which can be used as template to prepare one-dimensional nanostructured materials (metal nanowires) on the surface [23]. For this reason, a preliminary study of the electrodeposition of Cd–Ag crystals on HOPG could be useful, as a first stage, to fabricate a sensor for nitrate anions based on Cd–Ag nanowires in the near future [24].

In addition to experimental studies, theoretical analysis related to the surface alloy phenomena was found in the literature for different metals like Bi, Pt, Pd, and Sb deposition on Ag(111) [25–28]. Particularly, the Cd–Ag system has also been studied theoretically, establishing the most stable structures for bulk alloys at different Cd and Ag compositions [29, 30]. Only, in a recent work, a study of the surface alloy formation on Ag surfaces with Cd adatoms employing density functional theory (DFT) calculations was presented [31]. The proposed model is suitable in a scenario where both cations (Cd^{2+} and Ag^{+}) are contained in the same solution; however, in conditions where the metal ions are in different electrolytes, the expected mechanism according to experimental works corresponds to a vertical exchange process [18, 20]. In order to take into account this effect, some modifications of this model will be necessary.

The aim of this work is to explore the Cd UPD on Ag nanoparticles supported on HOPG and the involved alloy formation, comparing these results with those obtained in our previous report for the Cd–Ag/VC system [22]. Ex situ atomic force microscopy (AFM) analysis was used for the morphological characterization of the Cd–Ag bimetallic nanoparticles. The Cd UPD on Ag deposits was verified by cyclic voltammetry and the surface alloy formation was analyzed by desorption spectra using different polarization times. Furthermore, a theoretical study, employing DFT, was carried out to get more insight into the mechanism of the alloy process. An adequate model for the used experimental conditions, considering a site exchange mechanism between Cd and Ag, was applied, and the involved formation energy was evaluated.

Experimental and theoretical model

Highly ordered pyrolytic graphite (HOPG) (SPI Supplies, USA) inserted into a Teflon holder, with an exposed area of 0.2165 cm^2, was used as working electrode. Prior to each experiment, the substrate surface was prepared cleaving the first layers with an adhesive tape.

The solutions used for metal depositions were 1 mM Ag_2SO_4 + 0.1 M Na_2SO_4 (pH = 2) and 2 mM $CdSO_4$ + 0.1 M Na_2SO_4 (pH = 2.42), whereas a 0.1 M Na_2SO_4 (pH = 2.46) solution was employed as blank electrolyte. All of them were prepared with ultrapure chemicals (E. Merck, Darmstadt) and tri-distilled water. Prior to each experiment, the solutions were deaerated by nitrogen bubbling.

Electrochemical measurements were performed in a standard three-electrode electrochemical cell using a $Hg/Hg_2SO_4/K_2SO_4$ saturated electrode (SSE) and a platinum sheet as reference and counter-electrode, respectively. All potentials in this study are referred to the SSE. The experiments were performed with an EG&G Princeton Applied Research Model 273A potentiostat/galvanostat controlled by a microcomputer. The characterization of Ag and Cd/Ag deposits were carried out with a standard Nanoscope III AFM microscope (Digital Instruments, Santa Barbara, CA, USA) operated ex situ in contact mode using a scanner of 15 μm and oxide-sharpened silicon nitride probes with 5–40 nm nominal radius (Veeco Probes), with a spring constant of 0.06 N m^{-1}.

DFT calculations were performed using Vienna ab initio simulation package (VASP) [32–35], including the projector augmented wave (PAW) [36, 37] potentials. Parameters such as energy cut-off and k-points set were optimized. The Methfessel-Paxton first-order smearing approach [38] was used for all calculations, to describe the partial occupations of the electronic states near the Fermi level, with a smearing width of 0.2 eV. For the exchange correlation potential, the generalized gradient approximation (GGA) of Perdew, Burke, and Ernzerhof (PBE) [39] was employed. The k-points mesh was adjusted depending on the analyzed structure, using Monkhorst-Pack method [40]. For the unit cell, a cut-off energy value of 400 eV for the plane waves basis set, and a 13×13×13 k-point grid to sample the Brillouin zone, was enough for the total energy to converge within 10 meV.

Results and discussion

Electrodeposition of Cd on Ag nanoparticles

Prior to the formation of Cd–Ag bimetallic particles on HOPG surfaces, the electrodeposition process of the individual metals (Ag and Cd) was qualitatively evaluated by cyclic voltammetry, using separated electrolytes containing the corresponding metal cations. The voltammetric response is presented in the supplementary material (Fig. S1) and shows a typical behavior of a 3D nucleation and growth process controlled by diffusion. In both voltammograms, a cathodic/anodic current density peak associated with the metal deposition/dissolution is observed. These results are in agreement with those reported by other authors for Ag/HOPG [3, 41] and Cd/VC [22] systems. Furthermore, since the electrodeposition of Ag on HOPG begins at sufficiently more negative potential values, it is possible to carry out the generation of Ag particles and subsequently, the deposition of Cd on the pre-deposited Ag crystals, without dissolving them.

In order to investigate the electrodeposition of Cd on Ag crystals previously deposited on the HOPG electrode, cyclic voltammetric measurements were performed, and the obtained results are presented in Fig. 1. Ag deposits were obtained on the HOPG substrate applying a single potentiostatic pulse at $E = -0.214$ V vs SSE during $t = 10$ s. A cyclic voltammogram of the HOPG/Cd^{2+} system was included for comparison. Voltammetric results show that, during the negative scan, the current becomes increasingly negative, due to the electrodeposition of Cd on the HOPG-modified electrode, whereas a large anodic current peak is observed in the reverse scan, corresponding to the dissolution of this deposit. On the other hand, a small negative current at a potential more positive than the equilibrium potential of the 3D Cd bulk phase (E_{3DCd}) is also observed, which can be assigned to the Cd UPD on Ag particles. The equilibrium potential was calculated by Nernst equation for the employed solution giving a value of $E_{3DCd} = -1.12$ V vs SSE. The previous hypothesis is very important since a selective Cd deposition on the preexisting Ag nanocrystals could be achieved. From this figure, it is also evident that the electrodeposition of Cd on HOPG begins at potential values more negative than $E = -1.12$ V vs SSE, corroborating this assumption.

In order to analyze in more detail the Cd UPD on Ag nanoparticles, the process was evaluated in the potential range $-1.14 \leq E/\text{V vs SSE} \leq 0.40$. Figure 2 shows the voltammetric behavior of the HOPG/Ag(nanoparticles)/2 mM $CdSO_4$ + Na_2SO_4 0.1 M (pH = 2.42) system. The occurrence of an adsorption current density peak at about $E = -1.07$ V vs SSE, prior to that corresponding to the metal bulk deposition, can be distinguished more precisely. This peak could be associated to the Cd UPD on the previously deposited Ag crystals on the HOPG substrate.

The last assumption is based on the fact that this adsorption peak is located in the potential range where the Cd UPD on Ag(111) and Ag(100) macroelectrodes occurs, i.e., $-1.15 \leq E/\text{V vs SSE} \leq -0.75$ [18, 19]. These systems exhibit four and three adsorption/desorption peaks pairs, respectively, indicating that the Ag nanoparticles qualitatively show a different adsorption behavior with respect to Ag single crystals. However, more similar features were observed when a polycrystalline Ag electrode was used [42]. Mech et al. investigated the Cd UPD on a polycrystalline Ag electrode obtained by evaporation of Ag on glass substrates, and the voltammetric

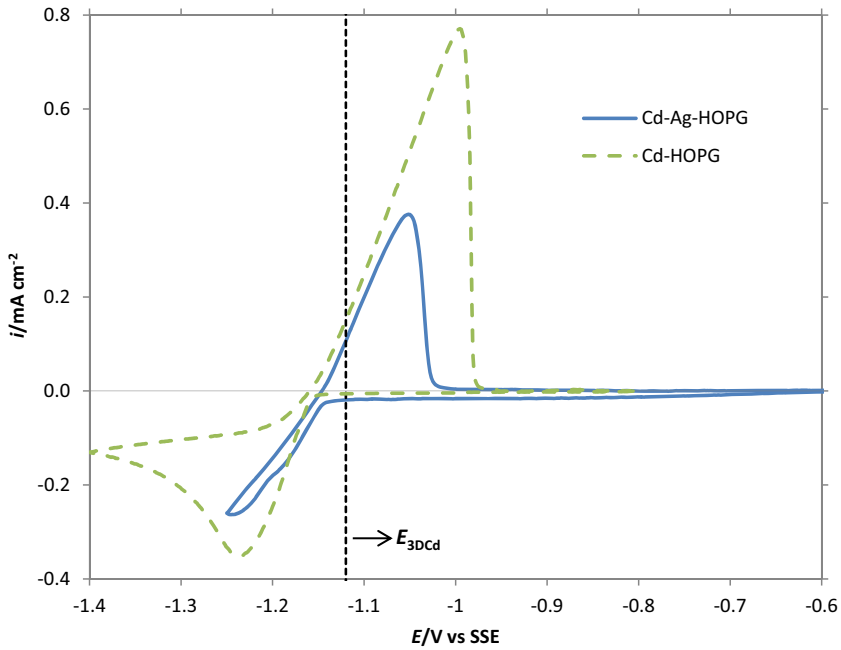

Fig. 1 Cyclic voltammetry of the systems HOPG/Ag(nanoparticles)/2 mM $CdSO_4$ + 0.1 M Na_2SO_4 (pH = 2.42) and HOPG/2 mM $CdSO_4$ + 0.1 M Na_2SO_4 (pH = 2.42). $dE/dt = 10$ mV s^{-1}

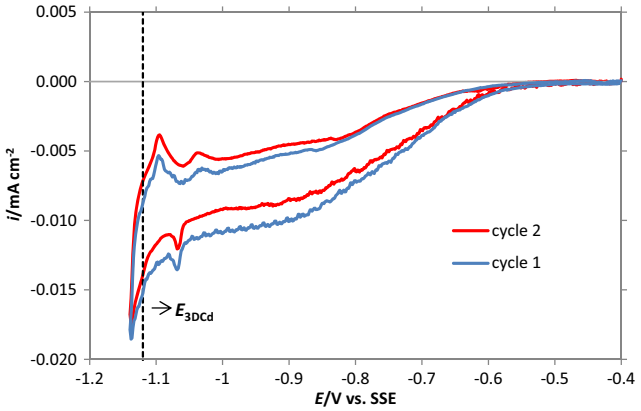

Fig. 2 Cyclic voltammetry of the Ag(nanoparticles)/HOPG-modified substrate in the UPD region. Solution: 2 mM $CdSO_4$ + 0.1 M Na_2SO_4 (pH = 2.42), dE/dt = 10 mV s^{-1}

results performed in the same solution as in this work, revealed that the Cd UPD is evidenced by a small shoulder starting at E = −0.859 V vs SSE and a very small peak around E = −1.109 V vs SSE. The authors suggested that these peaks can be attributed to the adsorption of an expanded Cd layer and subsequently a phase transformation to a closely packed monolayer, respectively [18, 19, 42]. Furthermore, the voltammogram, shown in Fig. 2, is slightly different to that obtained for Ag(nanoparticles)/VC electrodes [22], because the shoulder suggested by Mesh et al. [42], as well as the desorption peak of Cd UPD phases, are more easily distinguishable. This fact is probably related to some structural changes occurring on Ag nanoparticles by using a substrate with different structures.

During the anodic sweep, it is evident from the voltammetric measurements (Fig. 2), the corresponding dissolution peaks of the deposits generated in the overpotential deposition (OPD) and UPD ranges, respectively. It should be noted that, when the potential sweep is reversed in the anodic direction, a net positive current should be evident by the dissolution of previously adsorbed Cd particles if only a process of adsorption/desorption takes place. However, even though the two dissolution peaks of Cd deposits are observed, the current density remains negative. This behavior may be related to the hydrogen evolution reaction that occurs simultaneously with the Cd electrodeposition process, as it was tested in a 0.1 M Na_2SO_4 (pH = 2.46) blank solution (data not shown). These results are in agreement with those obtained by Miragliotta and Furtak [43] for the system Zn/Ag(111), using the second harmonic generation technique. Taking into account that Zn has a comparable electronic configuration to that of Cd, with a complete layer constituted by s and d orbitals, the behavior is expected to be similar. The authors observed the Zn UPD phenomenon on Ag(111) substrates, and from an analysis of Zn overlayers structures on Ag(111) as functions of the coverage and applied potential, they suggested that hydrogen is competing for surface sites preventing the Zn to fill all the sites in the UPD region.

In the second cycle (also included in Fig. 2), the cyclic voltammogram is shifted to more positive current values. This fact could be explained as a result of changes in the surface during the deposition process, related to the formation of a surface alloy between Cd and Ag. In this process, the Cd adlayer formed on Ag deposits is not stable and undergoes transformations involving a place exchange between Cd adatoms and surface Ag atoms. This interdiffusion process provides new sites for the adsorption of other Cd atoms on the surface. Consequently, the presence of more Cd generates a greater inhibition of the hydrogen reaction (higher overpotentials) during the second cycle, and shifts the current to more positive values. The latter hypothesis is supported by several publications found in the literature [15, 17–19, 22, 44], which predict the formation of a Cd–Ag alloy.

In order to get a better insight on the voltammetric behavior observed for the HOPG/Ag(nanoparticles)/Cd^{2+} system (Fig. 2), a film of Ag on HOPG was performed, trying to reproduce the surface of a Ag massive electrode on which the Cd deposition takes place. The Ag film was obtained by applying the following polarization routine: a cathodic sweep in a 1 mM Ag_2SO_4 + 0.1 M Na_2SO_4 (pH = 2) solution, in the potential region −0.45 ≤ E/V vs SSE ≤ 0.20, with dE/dt = 10 mV s^{-1}, and subsequently a potential step at E = −0.214 V vs SSE for 5 min. This modified substrate was then immersed in the solution containing Cd^{2+} ions. Figure 3 exhibits the voltammetric response of Cd UPD on the HOPG substrate modified with an Ag film, obtained at different scan rates. By increasing the scan rate, an increase of the Cd adsorption/desorption existing current peaks is observed. The first adsorption peak, relatively wide, at about E = −0.89 V vs SSE, is more clearly evidenced, which is associated to the adsorption of Cd expanded monolayers, as it was pointed out before. In the case of Cd adsorption on Ag nanoparticles, this process can be related with the shoulder starting approximately at E = −0.80 V vs SSE

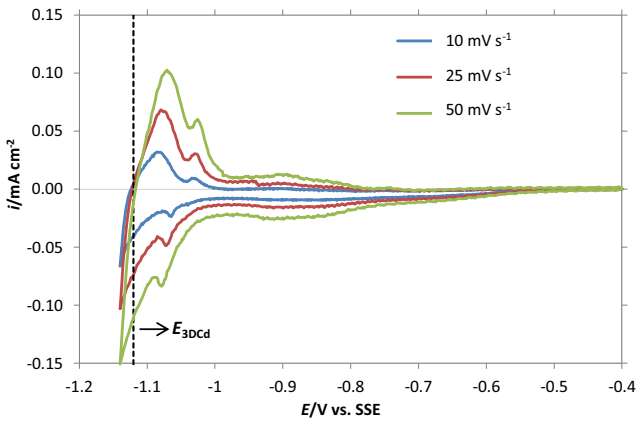

Fig. 3 Cyclic voltammetry in the UPD region of the HOPG substrate modified with an Ag film in 2 mM $CdSO_4$ + 0.1 M Na_2SO_4 (pH = 2.42) solution, at different scan rates

(c.f. Fig. 2). In consequence, the next small peak exhibited for an Ag film (Fig. 3) could be related to that observed for Ag nanoparticles at the same potential region. Therefore, this analysis corroborates that the adsorption peak corresponds to the phase transition of the expanded adlayer to a condensed Cd monolayer. Finally, the peak located at more negative potentials, corresponds to the Cd bulk deposition.

Morphological characterization of Cd–Ag nanoparticles

Structural information of the Ag deposits formed on HOPG was obtained from ex situ AFM studies. Ag deposits were obtained on the HOPG substrate in the same way as in the previous experiment. This electrode was then removed from the plating solution, rinsed with tri-distilled water and dried with hot air prior to the characterization using ex situ AFM. Figure 4a shows a representative AFM image of Ag nanoparticles on the HOPG substrate. The Ag deposits are distributed preferably on the step edges of the HOPG surface with a similar particle size, indicating an almost instantaneous nucleation mechanism with a 3D growth. On the contrary, although the electrodeposition of Ag on a VC electrode also follows a 3D nucleation and growth process controlled by diffusion, Ag deposits showed small differently sized Ag nanocrystallites uniformly distributed over the substrate, related to a progressive nucleation mechanism [1], evidencing the influence of the substrate structure.

Then, the modified HOPG substrate was introduced in the solution containing Cd^{2+} ions, generating Cd crystals by a potentiostatic pulse at $E = -1.14$ V vs SSE during 500 s. The potential (slightly more negative than E_{3DCd}) was selected in such a way to avoid Cd electrodeposition on HOPG, being possible due to the high affinity between the metals. The morphology of the generated Ag–Cd deposits is shown in Fig. 4b. It is observed that the Cd deposition on the modified electrode increases the size of the existing particles, without introducing significant morphological changes. The corresponding statistics of the detailed size distributions are presented in the supplementary material (Table S1 and Fig. S2). Taking into account that the diameter of the particles, as it is well known, may be influenced by the diameter and morphology of the AFM tip, a cross-sectional analysis on the marked line in the AFM images was carried out in order to compare the particles height on both modified substrates. The height difference observed in those sections is in the order of 2 nm, suggesting that Cd is deposited selectively on the Ag nanoparticles. Measurements on different areas of the electrode corroborated this assumption.

Cd–Ag alloy formation

Finally, in order to ascertain the occurrence of a surface alloy formation, in the Cd–Ag bimetallic par, desorption curves of the Cd–Ag/HOPG system for different polarization times, t_p,

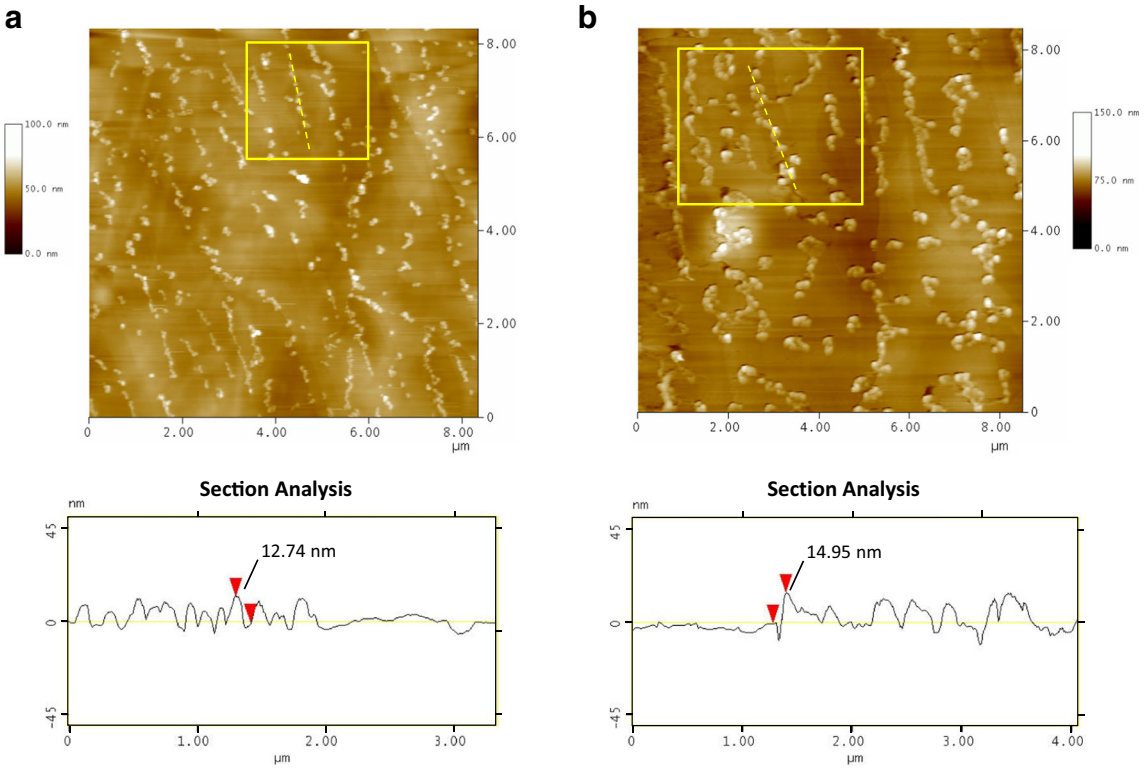

Fig. 4 **a**, **b** Ex situ AFM images of **a** Ag and **b** Cd–Ag particles on HOPG surfaces, with the corresponding sectional analysis

were performed. This method is commonly used to study alloy formation during the UPD process because this phenomenon can be recognized by the appearance of new desorption peaks at relatively high underpotentials together with changes in the normal desorption peaks [20, 21]. In a first step, the Ag deposit was obtained by a simple potentiostatic pulse at $E = -0.214$ V vs SSE during 10 s. Then, the modified electrode was immersed in the solution containing Cd^{2+} ions, where it was polarized at $E = -1.15$ V vs SSE for different t_p. After each polarization routine, an anodic sweep was carried out to obtain the corresponding desorption spectra, which are plotted in Fig. 5.

Three desorption peaks are exhibited in the figure, similarly to the results obtained for bimetallic Cd–Ag nanoparticles supported on VC substrates [22]. The shift of the first two peaks to more positive potential values, and the appearance of a third one at about −0.4 V with increasing polarization time, could indicate the occurrence of surface transformations associated with the alloying between Ag and Cd, as it was suggested by García et al. for the $Ag(111)/Cd^{2+}/SO_4^{2-}$ system [18]. The first peaks are mainly related to the dissolution of Cd OPD and UPD deposits on Ag nanoparticles, respectively. The shift of the first one to more positive potential values may be related to the previous formation of an alloyed phase between surface Ag atoms and adsorbed Cd atoms, during polarization. Consequently, since the Cd–Ag interaction energy in the surface layer becomes stronger than that for Cd–Cd, as expected for metals that present UPD [20], more positive potential values are required to dissolve Cd deposits. The same behavior is observed for the second peak, which is assigned to the Cd UPD dissolution. In the same way, the underpotentially deposited Cd adlayer is modified, during the polarization time, by interdiffusion of Ag and Cd atoms. Hence, this peak corresponds not only to the dissolution of the pure Cd adlayer formed by UPD but also to some surface alloy phase that is dissolved at this potential value. Finally, the new peak observed at more positive potential values and long polarization times could be attributed to the dissolution of a more stable Cd–Ag alloyed phase. This behavior is also in accordance with that obtained for the Zn/Ag system, from voltammetric and potentiostatic pulse measurements, complemented with X-ray diffraction analysis [45]. It was demonstrated that at least two alloyed phases were formed by diffusion of adsorbed Zn atoms into the Ag substrate.

Preliminary XPS analysis for the Cd–Ag/HOPG system is further evidence of alloy formation between both metals [46]. The spectra obtained for the Ag and Cd elements indicated that the doublets corresponding to the Ag 3d and Cd 3d regions exhibit a shift to higher energies (approximately 1 eV) with respect to the values reported in the literature for reduced and oxidized species of both metals, compatible with the alloy formation. In situ STM investigations are now in progress in order to observe if topography changes are evidenced on the particles after anodic stripping related to this surface alloy formation.

On the other hand, DFT calculations were performed to investigate the feasibility of forming a surface alloy between Cd and Ag on Ag surfaces. As it was previously mentioned, several publications found in the literature [15, 17–19] predict the formation of an alloy between these metals using experimental techniques. In these works, during the Cd UPD process on mono- and polycrystalline Ag electrodes, the formed Cd adlayer undergoes transformations due to the formation of a surface alloy between both metals. The first stage of the surface alloy formation, which is usually the rate determining step [20], involves a place exchange between surface Ag atoms and Cd adsorbed atoms, and then, the subsequent alloy film growth by interdiffusion of the metals [20]. This mechanism was proposed and modeled for Cd–Ag surface alloy formed on Ag massive electrodes [15, 18, 20], representing on one side the Cd deposits in the UPD regime, and on the other the Ag layer of the substrate. Also, as it was mentioned

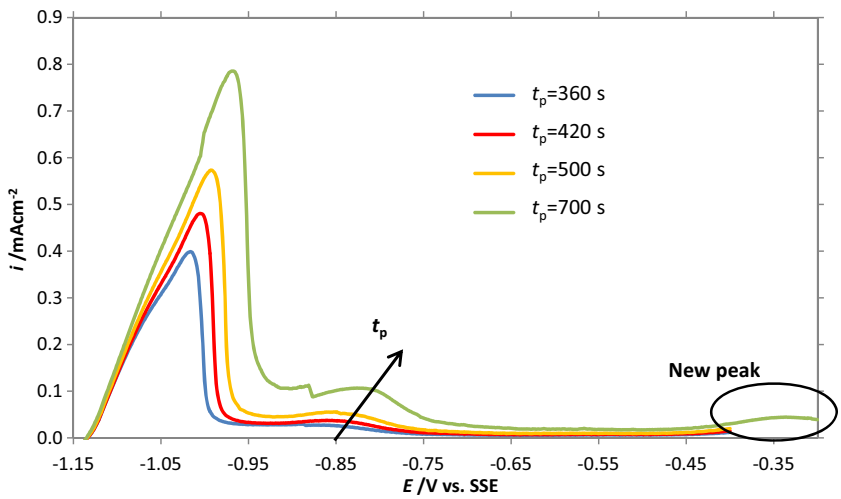

Fig. 5 Desorption spectra of the system HOPG/Ag(nanoparticles)/Cd^{2+} obtained at different polarization times, t_p. Solution: 2 mM $CdSO_4$ + 0.1 M Na_2SO_4 (pH = 2.42), dE/dt = 10 mV s^{-1}

on the introduction, a first attempt to quantify the surface alloying on Ag surfaces was carried out using DFT methods [31]. The model used in that work, contemplates a substitution mechanism of atoms in the surface to evaluate the formation energy of the surface alloy. However, as a site exchange mechanism between Cd and Ag is more probable to occur, the formation energy was evaluated in the new model, taking into account this process.

The theoretical analysis was focused in the formation of surface alloy on Ag(111) and Ag(100) surfaces. Despite the experimental results obtained in this work are related to nanoparticles, a theoretical analysis of Cd on both Ag facets is also representative to predict what would occur on them. This assumption can be done because both are low-index surfaces of fcc structures, like Ag bulk, with a high density of atoms. Thereby, they are surfaces which grow predominantly as a consequence of their low surface energy [20, 47]. The parameters used for DFT calculations were detailed in the theoretical model section.

The structure of Ag(111) and Ag(100) surfaces and the alloys formed between Ag and Cd were modeled, using a slab approach which repeated periodically in x, y, and z directions, with six layers, five of Ag and one of Cd, and a region of approximately 10 Å of vacuum in the z direction, to ensure that no interactions exist between periodic images of the slab. The number of layers was selected based on the previous work [31]. Different structures of two-dimensional (2D) Ag–Cd alloy were considered, i.e., 2×1, $\left(\sqrt{3} \times \sqrt{3}\right)$ R30°, 2×2, $\left(\sqrt{19} \times \sqrt{19}\right)$ R19° and 3×3 for Ag(111), and $\left(\sqrt{2} \times \sqrt{2}\right)$ R45°, 2×2 and 3×3 structures for the unit cell of Ag(100). These structures indicate the length of the lattice vectors of the surface alloy unit cell, with respect to the lattice vectors of the primitive cell of the Ag(111) and Ag(100) surfaces. The lattice vectors of the 2D alloy localize the Cd atoms in the Ag surface, as was proposed by other authors [28, 48, 49]. In this study, the surface alloy was formed by a place exchange of the adsorbed Cd atoms and the Ag surface as it is showed schematically in Fig. 6a. Each structure for the surface alloy corresponds to a different Cd concentration (C_{Cd}) in the first and second layer, after atom place exchange. Thus, we refer to a particular structure in terms of $C_{Cd,}$ defined as the ratio between the number of Cd atoms in the first layer and the total number of atoms in this layer.

All the structures were relaxed by minimizing the total energy of the unit cell using a conjugated gradient algorithm [50]. The formation energy of surface alloy by vertical exchange of the atom positions was evaluated by the equation:

$$\boldsymbol{E}_{\mathrm{f}} = \left(\boldsymbol{E}_{\mathrm{Cd}/surf\ \mathrm{Ag}} - \boldsymbol{E}_{surf\ \mathrm{Ag}} - \boldsymbol{n}_{\mathrm{Cd}}\boldsymbol{E}_{\mathrm{Cd}} + \boldsymbol{E}_{\mathrm{int}}\right)/\boldsymbol{n}_{\mathrm{Cd}} \qquad (1)$$

where $\boldsymbol{E}_{\mathrm{Cd/surf\ Ag}}$ is the energy of Ag surface with a monolayer of adsorbed Cd, $\boldsymbol{E}_{\mathrm{surf\ Ag}}$ is the energy of the clean Ag surface slab, $\boldsymbol{E}_{\mathrm{Cd}}$ is the energy of an isolated Cd atom, and $\boldsymbol{n}_{\mathrm{Cd}}$ is the number of adsorbed Cd atoms. $\boldsymbol{E}_{\mathrm{int}}$ represents the gain (negative) or lose (positive) of energy due to the exchange processes, obtaining this energy by differentiation of the energy of the structures schematically represented in Fig. 6a. The nomenclature I-AgCd was used to make reference of the exchange processes, adding on the right side, the place where the Cd monolayer is adsorbed on Ag surfaces, i.e., T- and H-hcp for Top and Hollow hcp sites, respectively, for Ag(111). In the case of Ag(100), the hollow site is represented by H only, because a unique hollow site exists for this surface. According to Eq. 1, a more negative value of the alloy formation energy by place exchange corresponds to a more favorable situation.

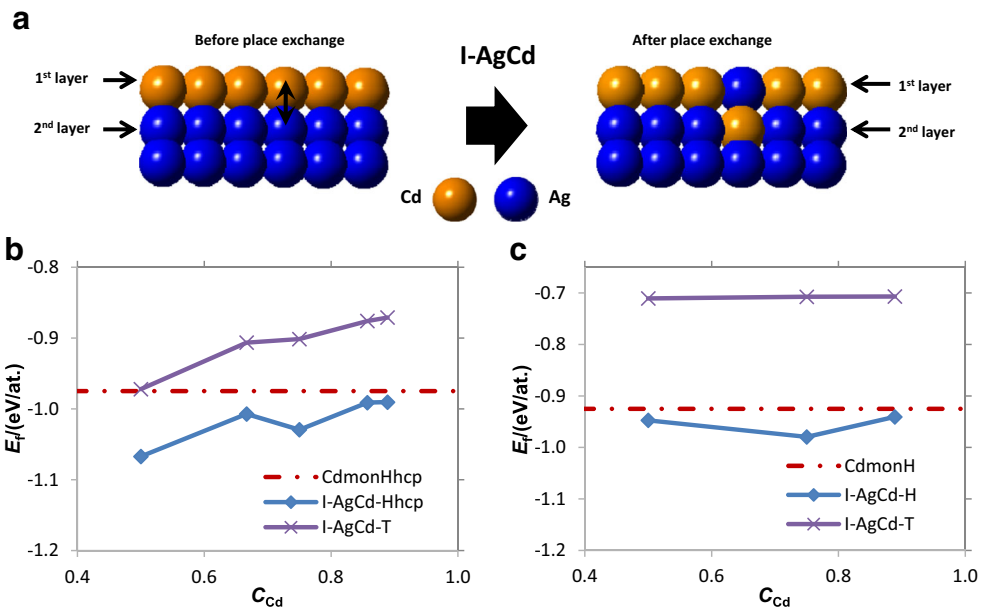

Fig. 6 **a–c** **a** Scheme of alloy formation by site vertical exchange mechanism. Surface alloy formation energy corresponding to different C_{Cd}, for **b** Ag(111) and **c** Ag(100) surfaces. The adsorption energy of a monolayer in the most stable site was represented in both cases with a *dotted line*

Additionally, with the aim to validate the pseudopotentials used, a Ag lattice parameter of 4.154 Å was obtained from bulk cell optimization using the same mentioned computational parameters, which overestimates 1.6% of the experimental value of 4.09 Å [51]. Also, the binding energy calculations for Ag–Ag and Cd–Cd dimers were performed, obtaining energy values of −1.750 and −0.014 eV, respectively, in good agreement with experimental values [52]. Likewise, the Cd–Ag binding energy of Ag–Cd dimer is −0.340 eV, having an intermediate bond strength between those of the pure metals, as expected for systems that present UPD [20].

The calculated formation energies of the structures considered, corresponding to different C_{Cd}, are shown in Fig. 6b. The formation energy of a monolayer of unitary coverage on the H-hcp site, was represented in the graph with a dotted line. The H-hcp site was determined as the most stable position for the adsorption of Cd on Ag(111) surface with a value of −0.975 eV/atom. This value was calculated with Eq. 1, neglecting the atomic exchange term. The results indicated that, for H-hcp sites, the alloy formation energy by vertical exchange sites is more negative (more stable) than the formation energy of a Cd monolayer. Therefore, a surface alloy formed by this mechanism is possible during the adsorption of Cd on the surface. In Fig. 6c, the results obtained for a Ag(100) surface indicate that the most stable site of adsorption is the hollow site (H), with an energy of $E = -0.925$ eV/atom. It is observed again that it is favorable to form a surface alloy by atomic exchange, when the monolayer is adsorbed on H site. Based on these calculations, it is easier to form a surface alloy on Ag(111) surface than on Ag(100).

On the other hand, it is also observed in Fig. 6b that E_f tends in general to increase at higher C_{Cd}. Bader charge [53] and projected density of states (PDOS) calculations were performed in order to explain this behavior. The analysis was focused in the structures 2×2 ($C_{Cd} = 0.75$) and $\left(\sqrt{3} \times \sqrt{3}\right)$ R30° ($C_{Cd} = 0.67$), which presented an unexpected change in comparison with the general tendency. The charge of Cd and Ag exchanged atoms, and their first neighbors were presented in Table S2 of the supplementary material. In all the cases, Cd transfers charge to Ag atoms, based on their charges sign. Also, Cd and Ag atomic charge values are higher than those obtained for adsorbed Cd monolayer on Ag surfaces (in the order of 0.07 to 0.09 e^- absolute values), showing a strong interaction between Ag and Cd when they are alloyed. However, there is not a significant charge difference between both alloy structures in order to explain the change on E_f.

The PDOS curves for both structures were obtained and presented in the supplementary material (Fig. S3). These curves show localized *d* states and dispersed *s* states over a wide range of energies. Again, a substantial variation is not evidenced when the C_{Cd} is modified, and therefore, we can conclude that the change on E_f does not correspond to a different orbital interaction. Accordingly, it is reasonable to suppose that the difference in stability with C_{Cd} is due to the proportion of Ag–Cd, Ag–Ag, and Cd–Cd bonds depending on the structure. Furthermore, as hollow sites were found to be favorable for Cd monolayer adsorption in order to form stable alloys (cf. Fig. 6b, c), an influence of the atomic stacking in the first layers could be inferred. Hence, returning to the particular case of $C_{Cd} = 0.75$ and $C_{Cd} = 0.67$, a balance of bonds in the first and second layer per unit area through the slab model was performed. The results corroborate that, although the number of Ag–Cd bonds does not change, the number of Cd–Cd and Ag–Ag bonds are higher for $C_{Cd} = 0.75$. Moreover, Ag atoms at this concentration are supported not only on two Ag and one Cd atoms, as for $C_{Cd} = 0.67$, but also on three Ag atoms. These effects produce that, at $C_{Cd} = 0.75$, the alloy structure becomes more stable.

Summarizing, the importance of the DFT calculations employed in this work lies in the fact that independently of other phenomena like adsorption of anions [18, 54, 55], the effect of the solvent and the electric field at the electrode interface of the electrochemical system [56], the interactions between Ag and Cd allow a place exchange between their atoms, which are favored by an electronic effect. Therefore, the theoretical results are another support to corroborate the tendency to form an alloy in this system. According to these results, the formation of surface alloy by vertical site exchange is sensitive to the site on the surface where the exchange occurs and the direction of the monocrystalline surface.

Conclusions

Bimetallic Cd/Ag particles were obtained on HOPG substrates by sequential electrodeposition of the metal components. Cd UPD process on Ag nanoparticles previously generated on HOPG was verified by cyclic voltammetry. This adsorption behavior is different from that observed for massive Ag electrodes and Ag particles supported on VC. The morphology of the metallic and bimetallic deposits was characterized by ex situ AFM. Initially, the images show Ag deposits of similar size distributed preferably on HOPG step edges. An increase of particle size after the electrodeposition of Cd is observed, but no remarkable morphological changes are evidenced on the surface, suggesting that Cd particles are deposited selectively over the Ag crystals previously deposited on HOPG. The influence of the hydrogen evolution reaction in the analyzed potential range was confirmed. The desorption spectra reveal dissolution peaks related to over- and under-potentially deposited Cd, and other phases which could be associated to the formation of an alloy between Cd and Ag particles. DFT calculations demonstrated the tendency of these metals to form surface alloy structures.

Acknowledgements The authors wish to thank the Universidad Nacional del Sur and CONICET (PIP-0853), Argentina, for financial support of this work. R. E. Ambrusi acknowledges a fellowship granted by CONICET.

References

1. Gunawardena G, Hills G, Montenegro I (1982) The electrodeposition of silver on vitreous carbon. J Electroanal Chem 138:241–254
2. Isse AA, Gottardello S, Maccato C, Gennaro A (2006) Silver nanoparticles deposited on glassy carbon. Electrocatalytic activity for reduction of benzyl chloride. Electrochem Commun 8:1707–1712
3. Pötzschke RT, Gervasi CA, Vinzelberg S, Staikov G, Lorenz WJ (1995) Nanoscale studies of Ag of silver electrodeposition on HOPG (0001). Electrochim Acta 40:1469–1474
4. Zoval JV, Stiger RM, Biernacki PR, Penner RM (1996) Electrochemical deposition of silver nanocrystallites on the atomically smooth graphite basal plane. J Phys Chem 100:837–844
5. Liu H, Penner RM (2000) Size-selective electrodeposition of mesoscale metal particles in the uncoupled limit. J Phys Chem B 104: 9131–9139
6. Liu H, Favier F, Ng K, Zach MP, Penner RM (2001) Size-selective electrodeposition of meso-scale metal particles: a general method. Electrochim Acta 47:671–677
7. Penner RM (2002) Mesoscopic metal particles and wires by Electrodeposition. J Phys Chem B 106:3339–3353
8. Zaleska-medynska A, Marchelek M, Diak M, Grabowska E (2016) Noble metal-based bimetallic nanoparticles: the effect of the structure on the optical, catalytic and photocatalytic properties. Adv Colloid Interf Sci 229:80–107
9. Darabdhara G, Sharma B, Das MR, Boukherroub R, Szunerits S (2017) Cu-Ag bimetallic nanoparticles on reduced graphene oxide nanosheets as peroxidase mimic for glucose and ascorbic acid detection. Sens Actuators B Chem 238:842–851
10. Fang W, Deng Y, Tang L, Zeng G, Zhou Y, Xie X, Wang J, Wang Y, Wang J (2017) Synthesis of Pd/Au bimetallic nanoparticle-loaded ultrathin graphitic carbon nitride nanosheets for highly efficient catalytic reduction of p-nitrophenol. J Colloid Interface Sci 490: 834–843
11. del Barrio MC (2007) PhD Thesis. UNS, Bahía Blanca
12. Ambrusi RE (2015) PhD Thesis. UNS, Bahía Blanca
13. Deutscher RL, Fletcher S (1990) Nucleation on active sites: part V. The theory of nucleation rate dispersion. J Electroanal Chem 277:1–18
14. Ng KH, Penner RM (2002) Electrodeposition of silver–copper bimetallic particles having two archetypes by facilitated nucleation. J Electroanal Chem 522:86–94
15. Bort H, Jüttner K, Lorenz WJ, Staikov G (1983) Underpotential alloy formation in the system Ag(hkl)/Cd^{2+}. Electrochim Acta 28: 993–1001
16. Jović VD, Jović BM, Despić AR (1990) The influence of solution composition on lead, cadmium and thallium underpotential deposition on (111) oriented silver single crystal surfaces. J Electroanal Chem 288:229–243
17. Jović VD, Jović BM (2002) Underpotential deposition of cadmium onto (111) face of silver from chloride containing solution. Electrochim Acta 47:1777–1785
18. García SG, Salinas DR, Staikov G (2005) Underpotential deposition of Cd on Ag(111): an in situ STM study. Surf Sci 576:9–18
19. Staikov G, García SG, Salinas DR (2010) 2D nucleation and growth phenomena in UPD of Cd on Ag(111) and Ag(100). ECS Trans 25:3–13
20. Budevski E, Staikov G, Lorenz WJ (1996) Electrochemical phase formation and growth. An introduction to the initial stages of metal deposition. VCH, Weinheim
21. Oviedo OA, Reinaudi L, García SG, Leiva EPM (2016) From fundamentals and theory to applications at the nanoscale. In: Scholz F (ed) Monographs in electrochemistry. Springer, Cham
22. Ambrusi RE, Staikov G, García SG (2014) Electrochemical synthesis of Cd–Ag bimetallic particles and the involved alloy formation. J Electroanal Chem 728:130–133
23. Walter EC, Murray BJ, Favier F, Kaltenpoth G, Grunze M, Penner RM (2002) Noble and coinage metal nanowires by electrochemical step edge decoration. J Phys Chem B 106:11407–11411
24. Murray BJ, Walter EC, Penner RM (2004) Amine vapor sensing with silver mesowires. Nano Lett 4:665–670
25. Woodruff D, Robinson J (2000) Sb-induced surface stacking faults at Ag(111) and Cu(111) surfaces: density-functional theory results. J Phys Condens Matter 12:7699–7704
26. Hyman MP, Loveless BT, Will Medlin J (2007) A density functional theory study of H_2S decomposition on the (111) surfaces of model Pd-alloys. Surf Sci 601:5382–5393
27. Hyman MP, Will Medlin J (2007) Effects of electronic structure modifications on the adsorption of oxygen reduction reaction intermediates on model Pt(111)-alloy surfaces. J Phys Chem C 111: 17052–17060
28. Mcleod IM, Dhanak VR, Matilainen A, Lahti M, Pussi K, Zhang KH (2010) Structure determination of the $p(\sqrt{3} \times \sqrt{3})$ R30° Bi-Ag(111) surface alloy using LEED I-V and DFT analyses. Surf Sci 604:1395–1399
29. Curtarolo S, Morgan D, Ceder G (2005) Accuracy of ab initio methods in predicting the crystal structures of metals: A review of 80 binary alloys. Calphad 29:163–211
30. Chouhan SS, Pagare G, Sanyal SP, Rajagopalan M (2012) First principles study on structural, electronic and elastic properties of AgX and AuX (X = Mg, Sc, Zn and Cd) intermetallic compounds. Comput Mater Sci 65:58–65
31. Ambrusi RE, García SG, Pronsato ME (2016) DFT study of the formation of Cd–Ag surface alloys on Ag surfaces. Comput Mater Sci 118:316–324
32. Kresse G, Hafner J (1993) Ab initio molecular dynamics for open-shell transition metals. Phys Rev. B 48:13115–13118
33. Kresse G, Hafner J (1994) Ab initio molecular-dynamics simulation of the liquid-metal-amorphous-semiconductor transition in germanium. Phys Rev. B 49(14):251–14,269
34. Kresse G, Furthmüller J (1996) Efficiency of ab initio total energy calculations for metals and semiconductors using a plane-wave basis set. Comput Mater Sci 6:15–50
35. Kresse G, Furthmüller J (1996) Efficient iterative schemes for ab initio total-energy calculations using a plane-wave basis set. Phys Rev. B 54(11):169–11,186
36. Blöchl PE (1994) Projector augmented-wave method. Phys Rev. B 50(17):953–17,979
37. Kresse G, Joubert D (1999) From ultrasoft pseudopotentials to the projector augmented-wave method. Phys Rev. B 59:1758–1775
38. Methfessel M, Paxton AT (1989) High-precision sampling for Brillouin-zone integration in metals. Phys Rev. B 40:3616–3621
39. Perdew JP, Burke K, Ernzerhof M (1996) Generalized gradient approximation made simple. Phys Rev. Lett 77:3865–3868
40. Monkhorst HJ, Pack JD (1976) Special points for Brillouin-zone integrations. Phys Rev. B 13:5188–5192
41. Ng KH, Liu H, Penner RM (2000) Subnanometer silver clusters exhibiting unexpected electrochemical metastability on graphite. Langmuir 16:4016–4023
42. Kowalik R, Żabiński P, Mech K (2013) Electrochemical studies of Cd UPD on polycrystalline silver. Electrochem Commun 31:49–51

43. Miragliotta J, Furtak TE (1989) Characterization of Electrodeposited Metals using Continuous-wave Optical Second-harmonic Generation. Surf Interface Anal 14:53–58
44. del Barrio MC, García SG, Salinas DR (2009) Alloy formation during the electrochemical growth of a Ag-Cd ultrathin film on Au(111). Electrochim Acta 55:451–457
45. Adžić G, McBreen J, Chu MG (1981) Adsorption and Alloy Formation of Zinc Layers on Silver. J Electrochem Soc 128: 1691–1697
46. Ambrusi RE, Sánchez MD, García SG (2017) Electrocatalytic effect of Ag and Cd bimetallic nanoparticles towards the reduction of nitrate and/or nitrite ions. Revista Máteria (in press).
47. Sholl DS, Steckel JA (2009) Density Functional Theory. A Practical Introduction. J. Wiley & Sons, Hoboken
48. Konvicka C, Jeanvoine Y, Lundgren E, Kresse G, Schmid M, Hafner J, Varga P (2000) Surface and subsurface alloy formation of vanadium on Pd(111). Surf Sci 463:199–210
49. Hirschl R, Hafner J (2002) First-principles study of Pd–V surface alloys I. Electronic structure of clean surfaces. Surf Sci 498:21–36
50. Press WH, Flannery BP, Teukolsky SA, Vetterling WT (1986) Numerical Recipies. Cambridge University Press, New York
51. Kittel C (1996) Introduction to Solid State Physics. J. Wiley & Sons, Hoboken
52. Morse MD (1986) Clusters of Transition-Metal Atoms. Chem Rev 86:1049–1109
53. Bader RFW (1990) Atoms in Molecules - A Quantum Theory. Oxford University Press, Oxford
54. Leikis D, Panin V, Rybalka K (1972) On the measurement of the electric double layer capacity at a polycrystalline cadmium electrode. J Electroanal Chem 40:9–12
55. Hamelin A, Vitanov T, Sevastyanov E, Popov A (1983) The electrochemical double layer on sp. metal single crystals: The current status of data. J Electroanal Chem 145:225–264
56. Bockris JO, Reddy AKN, Gamboa-Aldeco M (2002) Modern Electrochemistry: Fundamentals of Electrodics, Vol 2a. Kluwer Academic Publishers, Dordrecht